

Effects of Pixel Resolution, Mapping Window Size, and Spectral Species Classification on Remote Sensing of Plant Beta Diversity Using biodivMapR and Hyperspectral Imagery

Kevin Roberston¹, Eli M. Simonson¹, Natali R. Ramirez-Bullon¹, Benjamin Poulter², and Richard Carter³

¹Tall Timbers Research, Inc.

²NASA

³Valdosta State University

December 21, 2022

Abstract

Using imaging spectroscopy (hyperspectral imaging), we sought to assess the effects of image pixel resolution, size of mapping windows composed of pixels, and number of spectral species assigned to pixels on the capacity to map plant beta diversity using the biodivMapR algorithm, in support of the planned NASA Surface Biology and Geology (SBG) satellite remote sensing mission. BiodivMapR classifies pixels as spectral species, then calculates beta diversity as dissimilarity of spectral species among mapping windows each composed of multiple pixels. We used NEON airborne 1 m resolution hyperspectral images collected at three sites representing native longleaf pine ecosystems in the southeastern U.S. and aggregated pixels to sizes ranging from 1-90 m for comparative analyses. Plant community composition was groundtruthed. Results show that the capacity to detect plant beta diversity decreases with fewer pixels per mapping window, such that pixel resolution limits the size of mapping windows effective for representing beta diversity. Mapping window size in turn limits the spatial resolution of beta diversity maps composed of mapping windows. Assigning too few pixels per window, as well as assigning too many spectral species per image, results in overestimation of dissimilarity among locations that have plant species in common. This overestimation undermines the capacity to contrast mapping window dissimilarity within versus among community types and reduces the information content of beta diversity maps. These results demonstrate the advantage of maximizing spatial resolution of hyperspectral imaging instruments on the anticipated NASA SBG satellite mission and similar remote sensing projects.

Hosted file

952259_0_art_file_10540416_rmy9dn.docx available at <https://authorea.com/users/568326/articles/614214-effects-of-pixel-resolution-mapping-window-size-and-spectral-species-classification-on-remote-sensing-of-plant-beta-diversity-using-biodivmapr-and-hyperspectral-imagery>

1
2 **Effects of Pixel Resolution, Mapping Window Size, and Spectral Species**
3 **Classification on Remote Sensing of Plant Beta Diversity Using biodivMapR and**
4 **Hyperspectral Imagery**

5
6 **Kevin M. Robertson¹, Eli Simonson¹, Natali Ramirez-Bullon¹, Benjamin Poulter², and**
7 **Richard Carter³**

8 ¹Tall Timbers Research Station, Tallahassee, FL, USA

9 ²NASA Goddard Space Flight Center, Biospheric Sciences Lab., Greenbelt, MD, USA

10 ³Valdosta State University, Valdosta, GA, USA

11 Corresponding author: Kevin Robertson (krobertson@talltimbers.org)

12 **Key Points:**

- 13 • Ability to map plant beta diversity on landscapes using biodivMapR and similar
14 algorithms depends on having a sufficient number of pixels per mapping window.
- 15 • Increasing mapping window size to accommodate sufficient numbers of pixels per
16 window decreases spatial resolution of beta diversity maps.
- 17 • Assigning the appropriate number of spectral species is important for generating a
18 dissimilarity matrix that appropriately reflects actual plant beta diversity.

19

20 **Abstract**

21 Using imaging spectroscopy (hyperspectral imaging), we sought to assess the effects of image
22 pixel resolution, size of mapping windows composed of pixels, and number of spectral species
23 assigned to pixels on the capacity to map plant beta diversity using the biodivMapR algorithm, in
24 support of the planned NASA Surface Biology and Geology (SBG) satellite remote sensing
25 mission. BiodivMapR classifies pixels as spectral species, then calculates beta diversity as
26 dissimilarity of spectral species among mapping windows each composed of multiple pixels. We
27 used NEON airborne 1 m resolution hyperspectral images collected at three sites representing
28 native longleaf pine ecosystems in the southeastern U.S. and aggregated pixels to sizes ranging
29 from 1-90 m for comparative analyses. Plant community composition was groundtruthed.
30 Results show that the capacity to detect plant beta diversity decreases with fewer pixels per
31 mapping window, such that pixel resolution limits the size of mapping windows effective for
32 representing beta diversity. Mapping window size in turn limits the spatial resolution of beta
33 diversity maps composed of mapping windows. Assigning too few pixels per window, as well as
34 assigning too many spectral species per image, results in overestimation of dissimilarity among
35 locations that have plant species in common. This overestimation undermines the capacity to
36 contrast mapping window dissimilarity within versus among community types and reduces the
37 information content of beta diversity maps. These results demonstrate the advantage of
38 maximizing spatial resolution of hyperspectral imaging instruments on the anticipated NASA
39 SBG satellite mission and similar remote sensing projects.

40

41

42

43 **Plain Language Summary**

44 Mapping beta diversity, or the differences in species composition among different parts of a
45 landscape, is an important goal of satellite remote sensing. Different remote sensing products
46 have different sizes of pixels that make up the image, which can effect how much information
47 the image displays. NASA is interested in knowing the effects of image pixel size for designing
48 future satellite missions, including the upcoming Surface Biology and Geology (SBG) mission.
49 We used remote sensing data taken from aircraft at NEON research sites in the southeastern U.S.
50 to test how different pixel sizes, ranging from 1-90 m, affect how well beta diversity can be
51 mapped. We used the program biodivMapR, which creates maps from square "mapping
52 windows", which each contain multiple pixels that are classified according to their reflectance
53 data, and which are used to tell how different one mapping window is from the other. We found
54 that the larger the pixel size, the larger the mapping window has to be to have enough pixels to
55 map biodiversity well. The tradeoff is that larger mapping windows result in coarser biodiversity
56 maps. Using 30-45 m pixels, which has been recommended for the SBG mission, relatively large
57 areas covered by different natural community types can be distinguished, but smaller features
58 like isolated ponds and narrow streams may not be detected. The study shows the importance of
59 having image pixel sizes that are as small as possible, in addition to having high quality
60 information per pixel.

61

62 **1 Introduction**

63 The impact of human activities on the function and and sustainability of earth's biological
64 and physical systems places high priority on tracking global patterns of biodiversity and
65 ecosystem change. Given the high cost and limited geographic distribution of field plots for
66 ecosystem monitoring, remote sensing will play an increasingly important role in systematically
67 monitoring trends in biodiversity and ecosystem health. Remote sensing approaches depend on
68 demonstrated links between field-observed data and remotely sensed reflectance data in order to
69 develop automated systems for ecological interpretation of imagery covering wide geographic
70 areas (Pereira et al., 2017). The increasing availability of imaging spectroscopy, hereafter
71 hyperspectral imagery, in which hundreds of reflectance wavelengths are measured for each
72 pixel, promises a paradigm shift in the capacity to remotely monitor biodiversity (Schimel et al.,
73 2020). However, current application of hyperspectral technology remains limited by spatial and
74 temporal coverage (Cawse-Nicholson et al., 2021).

75 In light of these needs, the 2017-2027 Decadal Survey organized by the United States
76 National Academy of Sciences, Engineering, and Medicine (NASEM, 2018) established surface
77 biology and geology (SBG) as a designated observable using satellite remote sensing. The SBG
78 project is anticipated to use hyperspectral visible to shortwave infrared (VSWIR; 380-2500 nm)
79 imagery in a mission to be lead by the National Air and Space Administration (NASA) (Cawse-
80 Nicholson et al., 2021). To date, the Decadal Survey recommends a VSWIR instrument with 30-
81 45 m pixel resolution, as well as ≤ 16 day global revisit time and 10 nm spectral resolution in the
82 380-2500 nm range. During the current formulation phase, it is important to consider tradeoffs
83 among choices of parameter specifications. One important parameter under consideration is
84 spatial resolution of imagery, which may have a significant influence on the capability to

85 remotely sense spatial distributions of biodiversity (Gamon et al., 2020).

86 The current study focuses on implications of spatial resolution of imagery on
87 effectiveness of remotely sensing plant community beta diversity using the algorithm
88 biodivMapR (Féret and de Boissieu, 2020). Beta diversity refers to spatial variation, or turnover,
89 of species composition among plant communities at the landscape scale. BiodivMapR also
90 estimates alpha plant diversity (local diversity) as diversity of spectral species (classified pixels)
91 within larger mapping windows, which depends on the Spectral Variation Hypothesis (Palmer et
92 al., 2002; Rocchini et al., 2004), or the assumption that local variation in spectral signatures
93 among pixels corresponds to plant functional diversity and species diversity (Gamon et al.,
94 2020). However, as the size of pixels increasingly exceeds the size of individual plant species,
95 this assumption becomes much less certain (Féret and Asner, 2014; Féret and de Boissieu, 2020;
96 Rocchini et al., 2018). For example, in grasslands where there multiple species per m², this
97 relationship appears to break down at pixel sizes larger than about 5 m (Gholidezah et al. 2019;
98 2021; Gamon et al., 2020). Within the range of spatial resolutions suggested for the SBG mission
99 (30-45 m), alpha diversity procedures will likely not be effective in herb-dominated plant
100 communities such as those in the current study, which can have > 20 species per m² (Glitzenstein
101 et al., 2003). Remote sensing of beta diversity is less limited by spatial resolution, as pixels
102 classified as spectral species can represent local community composition instead of individual
103 species (Rocchini et al., 2018). Thus, the degree of similarity in biodiversity between two areas
104 of interest can be estimated by the similarity in spectral species composition. BiodivMapR uses
105 the spectral species concept (Rocchini et al., 2010) to calculate dissimilarity in spectral species
106 among larger mapping windows containing multiple pixels. In this light, biodivMapR might be
107 effectively applied for detection of plant beta diversity using ranges of image spatial resolution

108 recommended for the SBG mission and currently available from existing hyperspectral satellite
109 missions (e.g., PRISMA, DESIS).

110 The capacity to remotely sense beta diversity at spatial resolutions larger than individual
111 plants depends on the plant community concept, specifically that plant species belonging to
112 particular assemblages are adapted to certain environmental conditions (Lortie et al., 2004) and
113 collectively have definable reflectance characteristics (Cavender-Bares et al., 2020). Ability to
114 map beta diversity also depends on the pixel resolution of available imagery relative to the
115 spatial scale of plant community turnover (Gamon et al. 2020). Landscapes within the study
116 region, the southeastern U.S. Coastal Plain, provide a useful scenario for assessing methods of
117 detecting beta diversity, given their complex spatial arrangements at small spatial scales (Carr et
118 al. 2010), geologically active karst topography that influences community distribution (Lane and
119 D'Amico, 2010), strong responses of vegetation to slight elevation changes (Drewa et al. 2002),
120 and varying coverage and effects of frequent prescribed fire (Robertson et al. 2019), which
121 contribute to the region being recognized as a global biodiversity hotspot (Noss et al., 2015).
122 Thus, the ability to differentiate communities for mapping beta diversity will depend on both
123 image pixel size and dimensions of the mapping windows composed of pixels classified as
124 spectral species, among which dissimilarity of spectral species is calculated for mapping beta
125 diversity (Asner and de Boissieu, 2020). Larger mapping windows contain more pixels and
126 spectral species and thus have more refined capacity to estimate dissimilarity, but at the cost of
127 spatial resolution of the beta diversity map. Effective mapping of beta diversity may also be
128 influenced by the specified number of spectral species into which pixels are classified (Féret and
129 de Boissieu, 2020).

130 In this study, we use biodivMapR to compare estimates of beta diversity among levels of

131 image resolution ranging in pixel size from 1 m to 90 m. Our approach was to use 1 m resolution
132 imagery from airborne sensors at three National Ecological Observatory Network (NEON;
133 neonscience.org) sites representing different natural landscapes representative North American
134 Coastal Plain pine communities. We aggregated pixels to simulate coarser resolution imagery
135 and ran biodivMapR algorithms to assess its capacity to detect beta diversity using different pixel
136 resolutions using nearly constant sized mapping windows. We also explored the effects of
137 mapping window size and the number of assigned spectral species on the ability to distinguish
138 natural communities. We used field-collected data to confirm the similarity within and
139 dissimilarity among plant communities with regard to actual plant species composition and to
140 provide points of reference to estimates by biodivMapR. We use the results to discuss the
141 implications of spatial resolution requirements of imagery for measuring biodiversity on natural
142 landscapes using space-based hyperspectral imagery and indicate potential applications and
143 limitations of such imagery and to provide guidance for development of the anticipated SBG
144 mission.

145 **2 Materials and Methods**

146 2.1 Study Sites

147 We used remote sensing and field-collected plant presence and percent cover data
148 provided by NEON (2022) from sites at three properties representing different longleaf pine
149 (*Pinus palustris*) savanna ecosystems within the southeastern U.S. Coastal Plain. The properties
150 were the Disney Wilderness Preserve (DSNY), Jones Ecological Research Center (JERC), and
151 Ordway-Swisher Biological Station (OSBS) (Fig. 1). The sites were selected for the availability
152 of NEON airborne hyperspectral imagery with 1 m resolution acquired annually within a 10 km
153 x 10 km area centered on the property and the availability of surface vegetation data. Also, the

154 sites represent the three historically dominant upland ecosystems in the Coastal Plain region and
155 their associated community types, described below for each site.

156 2.1.1 Disney Wilderness Preserve (DSNY)

157 DSNY (28.1287°N, -81.4303°W) is a 4,600 ha property owned and managed by The
158 Nature Conservancy. Elevation of the property is approximately 15 m above sea level (asl), and
159 low to high average monthly temperatures are 15.6°C in January and 27.8°C in July. Native pine
160 savannas dominating the DSNY landscape are more specifically flatwoods pine savannas (FNAI,
161 2010), historically the most widespread

162 natural community in Florida. Soils are
163 mostly in the Spodosol order (Soil
164 Survey Staff 2022), which are sandy with
165 organic matter and saturated part of the
166 year. The flatwoods pine community has
167 sparse tree canopy dominated by longleaf
168 pine with an understory of evergreen
169 shrubs, especially saw palmetto (*Serenoa*
170 *repens*) and gallberry (*Ilex glabra*), and a

171 diverse herbaceous plant community
172 dominated by wiregrass (*Aristida*
173 *beyrichiana*) in most areas. It is

174 dependent on frequent prescribed fire (Glitzenstein et al., 2003), applied at three-year or shorter
175 intervals at DSNY. Cypress forests (syn. dome swamp, basin swamp; FNAI, 2010) occur at
176 slightly lower elevations with long hydroperiods and a nearly closed canopy of pond cypress

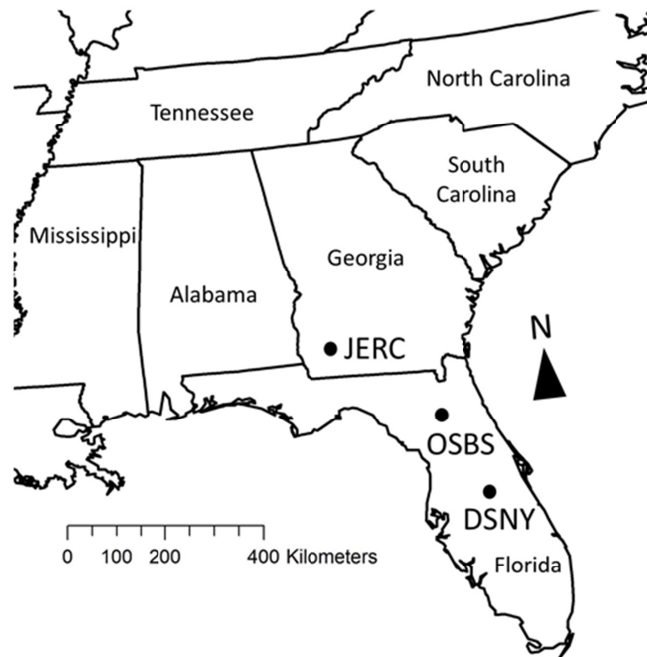


Figure 1. Locations of the three NEON study sites within the southeastern U.S.: Disney Wilderness Preserve (DSNY), Jones Ecological Research Station (JERC), and Ordway-Swisher Biological Station (OSBS).

177 (*Taxodium ascendens*) with evergreen shrubs and shade-tolerant herbs in the understory.
178 Evergreen wetland forests (syn. baygall; FNAI, 2010) occur in similar though often shallower
179 physical locations but are dominated by evergreen broadleaf trees, primarily titi (*Cyrilla*
180 *racemiflora*) and sweetbay (*Magnolia virginiana*). Grass marshes (syn. depression marsh, basin
181 marsh; FNAI, 2010) are herbaceous wetlands associated with shallow karst depressions with
182 fluctuating water levels. Scrub is composed of shrub-like trees with sparse herbaceous surface
183 vegetation in slightly raised areas of nearly pure sand, and they typically burn with crown fires
184 less frequently than flatwoods (FNAI, 2010). Native pastures are former flatwoods communities
185 where trees and most woody vegetation were removed but otherwise have similar herbaceous
186 vegetation and are frequently burned.

187 2.1.2 Jones Ecological Research Center (JERC)

188 JERC (31.2205°N, -84.4793°W) is a 12,000 ha private research center. Elevation ranges
189 from approximately 30-50 m asl. Low to high average monthly temperatures are 10.2°C in
190 January and 28.4°C in July. The dominant soils are in the Ultisol order (Soil Survey Staff, 2022),
191 consisting mostly of sand with a clayey subhorizon. Native pine savannas dominating JERC are
192 specifically upland pine communities (FNAI, 2010). This community type has an open canopy of
193 mostly longleaf pine and fire-tolerant broadleaf trees (mostly genera *Quercus* and *Carya*),
194 surface vegetation of resprouting broadleaf tree and shrub species, and a diverse herbaceous
195 community dominated by wiregrass in most areas (Carr et al., 2010). It is dependent on frequent
196 fire and is typically burned at two-year intervals at JERC. Bottomland forest communities occur
197 in occasionally flooded areas and have a closed-canopy dominated by mesic broadleaf deciduous
198 trees with shrubs and sparse shade-tolerant herbaceous plants in the understory (FNAI, 2010).
199 Old-field pine communities are former row crop sites that have been planted with longleaf pine

200 and managed with frequent fire similar to the upland pine savannas, such that it contains a subset
201 of native savanna plant species (Kirkman et al., 2004; Dixon et al., 2021). Cultivated crop sites
202 are annually tilled and planted mostly with cotton, peanuts, corn, or soybeans and harbor a
203 variety of agricultural weeds.

204 2.1.3 Ordway-Swisher Biological Station (OSBS)

205 OSBS (29.6903°N, -82.0176°W) is a 3,800 ha property owned and managed by the
206 University of Florida. Elevation of the property ranges from 30-55 m asl, and low and high
207 average monthly temperatures are 12.6°C in January and 27.6°C in August. The dominant soils
208 are in the Entisol order (Soil Survey Staff, 2022) consisting mostly of sand. Its native pine
209 community is specifically sandhill pine (FNAI, 2010) burned at three-year intervals. This
210 community has an open canopy of mostly longleaf pine and fire-tolerant broadleaf trees and
211 relatively xeric surface vegetation, though also dominated by wiregrass like the other sites. Open
212 wetland forests (syn. basin swamps; FNAI, 2010), with an open canopy of mostly pond cypress
213 and black gum (*Nyssa biflora*), occur in locations with long hydroperiods and have understory
214 vegetation consisting of wetland shrubs, ferns, and floating and emergent wetland herbaceous
215 vegetation. Upland mixed forests (syn. upland hardwood forest; FNAI, 2010) occupy areas that
216 were previously sandhill pine communities but fire-excluded for decades, resulting in a closed
217 canopy of oaks and residual pines and sparse understory vegetation. Disturbed areas are sandhill
218 pine communities with a history of intensive soil disturbance and are characterized by few pine
219 and broadleaf trees and sparse ruderal forbs and grasses. Bottomland forests and grass marshes at
220 OSBS are similar to those described for DSNY and JERC, respectively.

221 2.2 Field Data

222 We used field data to confirm that locations within areas classified as a particular

223 community type have similar plant species composition relative to other community types. We
 224 the plant presence and percent cover datasets provided for each site through the NEON portal
 225 (NEON, 2022), as well as plots that we established and censused on each of the properties, with
 226 the goal of providing multiple plots per common community type. Plots used in the study were
 227 distributed such that each represented an individual natural community feature or management
 228 unit. Both the NEON plots and our additional plots were 20 m x 20 m (400 m²) and were
 229 censused for presence of all vascular plant species during the growing season. The NEON plots
 230 had all been censused within the previous three years. We censused additional plots at DSNY in
 231 late March, OSBS in April, and JERC in May of 2022. We also field-validated our interpretation
 232 of community types at virtual plot locations chosen from aerial photography for selecting points
 233 representing those communities for the biodivMapR analyses, described below. For the dominant
 234 pine community types, total numbers of plots ranged from 20-27 among the three study sites, and
 235 for the other community types numbers of plots ranged from 2-12 (average = 6) (Table 1).

236 Table 1. Plant community types, numbers of field-measured plots (NEON plant presence and
 237 percent cover plots and our plots combined), and numbers of virtual plot locations remotely
 238 chosen for analysis for the three study sites. DSNY = Disney Wilderness Preserve, JERC = Jones
 239 Ecological Research Center, OSBS = Ordway-Swisher Biological Station.

Site	Community	Field plots	Virtual plots
DSNY	Cypress forest	2	5
DSNY	Evergreen wetland forest	2	6
DSNY	Flatwoods pine savanna	25	8
DSNY	Grass marsh	4	5
DSNY	Pasture	12	4
DSNY	Scrub	4	6
JERC	Bottomland forest	3	5
JERC	Cultivated crops	5	5

JERC	Old-field pine savanna	3	4
JERC	Upland pine savanna	26	6
OSBS	Bottomland forest	7	4
OSBS	Disturbed	5	6
OSBS	Grass marsh	10	6
OSBS	Open wetland forest	5	5
OSBS	Upland mixed forest	7	6
OSBS	Sandhill pine savanna	13	11

240

241 For each of the three sites, we ran nonmetric multidimensional scaling (NMS) ordinations
242 using PC-ORD v. 7 (McCune and Mefford, 2018) to confirm that communities are relatively
243 definable in terms of plant species composition. We also ran multi-response permutation
244 procedures (MRPP) based on the Bray-Curtis dissimilarity matrices, which averages the within-
245 community dissimilarity and total dissimilarity to calculate within-community agreement (A)
246 (McCune and Grace, 2002) for comparison to biodivMapR results, described below.

247 2.3 Airborne Hyperspectral Reflectance Data

248 Surface reflectance data were acquired by the NEON Imaging Spectrometer (NIS) on the
249 NEON Airborne Observation Platform (AOP) and accessed through the NEON Data Portal
250 (data.neonscience.org). The NIS design is based on Next Generation Airborne Visible/Infrared
251 Imaging Spectrometers (AVIRISng), which was developed under the Next-Generation Imaging
252 Spectrometer (NGIS) program at NASA's Jet Propulsion Laboratory (JPL). The raw data include
253 426 bands collected at 1-m spatial resolution in the visible-to-shortwave infrared (VSWIR)
254 range between 0.38 and 2.5 microns and a spectral sampling of 5 nm (Karpowicz and Kampe,
255 2015). Images were collected by NEON as flightlines approximately 500 m in width which were
256 mosaiced for the 10 km x 10 km area and subsequently separated into 1 km² tiles available for

257 download (Karpowicz and Kampe, 2015). We downloaded and mosaiced tiles to cover our area
258 of interest, with numbers of tiles ranging from 25 to 50 tiles among the three study sites.

259 Reflectance data used in this study were collected in September, 2021 for all three sites.
260 Although time since the previous prescribed fire no doubt had some influence on the reflectance
261 properties of fire-dependent communities, the time between burning in the spring and imaging in
262 September is sufficient for pine savannas to have considerable recovery by resprouting perennial
263 vegetation characteristic of these communities (Picotte and Robertson, 2011).

264 NEON reflectance data were initially converted from at-sensor radiances to surface
265 reflectance using the ATCOR atmospheric correction (Karpowicz and Kampe, 2015) and then
266 provided to the community as georectified images in ENVI format using the neonhs R package
267 (<https://www.earthdatascience.org/neonhs/>). No additional corrections were performed. For each
268 site, we mosaiced multiple 1 km x 1 km flightline mosaics provided by NEON to create a
269 seamless product that included most of the NEON vegetation plots. Finally, we used a python
270 script from the Space-based Imaging Spectroscopy and Thermal pathfinder (SISTER) resample
271 repository (<https://github.com/EnSpec/sister-resample>) to aggregate the NEON mosaics from
272 their native resolution of 1 m to 5 m, 15 m, 30 m, 40 m, 60 m, and 90 m. These final mosaics,
273 including the original 1 m resolution mosaic, served as the inputs into the biodivMapR package
274 (<https://jbferet.github.io/biodivMapR/index.html>).

275 R scripts provided through the GitHub page were used to guide the workflow. The first
276 step masked irrelevant pixels (e.g., non-vegetated, cloudy, shadow) based on a spectral
277 thresholding of NDVI and the Blue/NIR domains. We used the default thresholds for Blue and
278 NIR but lowered the Normalized Difference Vegetation Index (NDVI) threshold from the default
279 of 0.5 to 0.1 to include lightly vegetated areas characteristic of some frequently burned areas. A

280 series of processing steps were then applied to the remaining data, including band removal,
281 continuum removal, and dimensionality reduction using principal component analysis (PCA).
282 The wavelengths removed from the analysis corresponded to atmospheric water absorption or
283 otherwise had a high signal to noise ratio (Sousa et al., 2022), specifically 0-400 nm, 895-1005
284 nm, 1320-1480 nm, 1780-2040 nm, and 2400-3000 nm.

285 After the data were normalized and transformed, we performed a selection of principal
286 components that were most relevant to the mapping of biodiversity in our study areas. While
287 some components highlighted differences in vegetation properties, others showed information
288 related to sensor characteristics or very high noise level. Therefore, it was important to visualize
289 each component and follow the published recommendations for component selection (Féret and
290 de Boissieu, 2020). The next step partitioned the selected components into a predefined number
291 of clusters (spectral species) by using k-means clustering and assigned a cluster ID to each pixel.
292 We used either 50 spectral species (default) and then 20 spectral species for comparison,
293 described below. BiodivMapR then calculates the Bray-Curtis dissimilarity index for each pair of
294 mapping windows based on abundance of each spectral species, and then uses an ordination
295 technique to assign three numbers to each pixel as the basis for visualizing maps of beta
296 diversity. BiodivMapR can also provide a BC matrix including only dissimilarities among points
297 of interest, which we used for analyses described below.

298 In our first analysis, the goal was to test for effect of pixel size on the ability of
299 BiodivMapR to distinguish natural community types within each site in terms of dissimilarity in
300 spectral species in pairwise comparisons among locations within and among communities. For
301 this analysis, we used similarly size mapping windows (270-300 m) for comparison among pixel
302 resolutions, such that the number of pixels per mapping window varied by several orders of

303 magnitude (Table 2). We used reference real color imagery from NEON used to create virtual
 304 plots by placing points within homogeneous areas of a given community type large enough to
 305 contain one mapping window. We took this approach instead of using the locations of the 20 m x
 306 20 m plots with field data because of the spatial mismatch between the plots and the much larger
 307 mapping windows, and so we could choose a more balanced representation of community types
 308 than provided by the field plots (Table 2). However, we confirmed in the field that the virtual
 309 plot locations accurately represented the remotely interpreted community type. The function
 310 ‘biodiversity from plots’ was then used to extract the Bray-Curtis dissimilarity matrices
 311 comparing spectral species composition among mapping windows centered on the virtual plot
 312 point locations.

313 Table 2. Pixel resolution, square mapping window width, and number of pixels per mapping
 314 window used to calculate diversity metrics from NEON imagery.

Pixel size (m)	Window size (m)	Pixels per window
1	270	72,900
5	270	2,916
15	270	324
30	270	81
40	280	49
60	300	25
90	270	9

315

316 Using the Bray-Curtis dissimilarity matrices, we ran MRPP analyses using the vegan
 317 package and the function mrpp in R (Oksanen et al., 2022) to provide the average within-
 318 community dissimilarity and total dissimilarity for each study site and pixel resolution (Table 2)
 319 and using 50 versus 20 spectral species. From these values we calculated within community

320 agreement (A) as $A = 1 - (\text{average within variance} / \text{average total variance})$ (McCune and Grace,
321 2002). We also calculated the percentage of total dissimilarities equal to 1 (no spectral species in
322 common) to assess the method's ability to identify relative dissimilarity as opposed to absolute
323 dissimilarity. We charted trends in each of these metrics with increasing pixel size to visualize
324 the effects of image resolution on capacity to discriminate natural communities as reflected in the
325 A statistic.

326 In a second analysis, we assessed the effects of changing the sizes of the both pixel size
327 and mapping windows on ability to discriminate among community types. For this analysis, the
328 sizes of mapping windows were adjusted according to pixel size to maintain numbers of pixels
329 per window within the range of 49-81 (Table 3), which is within the 50-400 range recommended
330 by Féret and de Boissieu (2020). In this analysis we used 20 spectral species, as the first analysis
331 Table 3. Pixel resolution, square mapping window width, and number of pixels per mapping
332 window used to calculate diversity metrics from NEON imagery.

Pixel size (m)	Window size (m)	Pixels per window
1	8	64
5	40	64
15	120	64
30	270	81
40	280	49

333 revealed that this number provides higher resolution among community types. We used only
334 pixel sizes 1 m, 5 m, 15 m, 30 m, and 40 m, as larger pixel resolutions would require mapping
335 windows with 480 m or greater dimensions, which is larger than the area of any natural
336 community feature in the study. Similar to the first analysis, we ran MRPP analyses to derive
337 within community dissimilarity, total dissimilarity, the A statistic, and percentage of

338 dissimilarities equal to one, and
339 values were charted to visualize
340 trends among pixel sizes.

341 3. Results

342 NMS analyses of field
343 collected data generally confirmed
344 that community types were well
345 defined by their plant species
346 composition, represented by
347 presence or absence of species, as
348 visualized using NMS ordination
349 (Figure 2).

350 The analysis using varying
351 pixel resolutions (1-90 m) with
352 similar sized mapping windows
353 (270-300 m) showed a fairly strong
354 decrease in capacity to identify beta
355 diversity with increasing pixel size
356 (Figure 3). The average dissimilarity
357 among plots within community
358 types increased with coarser pixel
359 resolution (Figure 3a). Average total
360 dissimilarity among all plots also

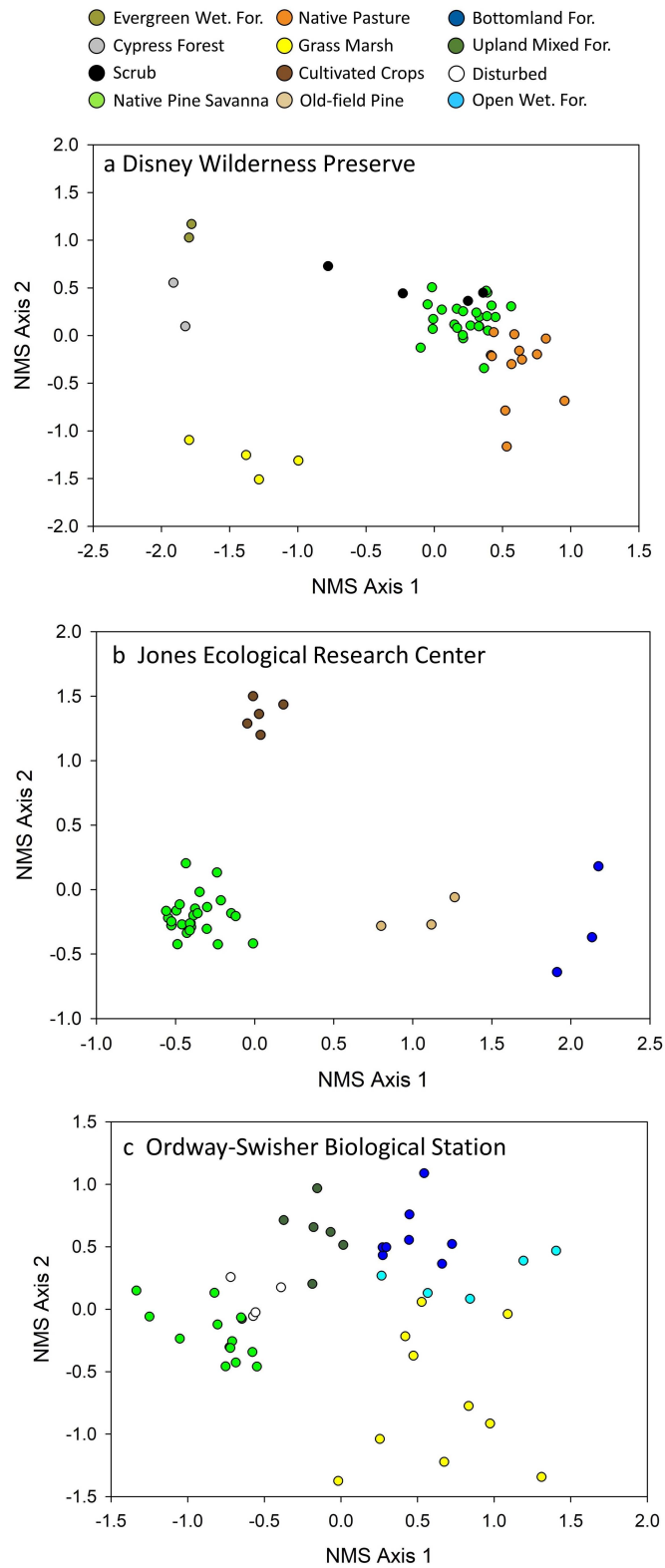


Figure 2. Results from NMS ordination on field collected plant species presence-absence data for each community type and study site. Symbols represent data from 20 m x 20 m field plots.

361 increased, but more gradually (Figure 3b).

362 These patterns resulted in a general

363 decrease in within community agreement (A

364 = 1 - (within dissimilarity / total

365 dissimilarity)) with coarser pixel resolution

366 (Figure 3c). The percentage of pairwise

367 comparisons with dissimilarity = 1 (no

368 spectral species in common) increased with

369 coarser pixel resolution (Figure 3d). These

370 patterns can also be visualized through

371 results of NMS analyses reflecting the

372 Bray-Curtis dissimilarity matrices

373 comparing spectral species among

374 communities (Figure 4a-i). Plant

375 communities generally can be distinguished

376 in the ordination plots using 1 m pixels

377 (Figure 4a-c) and 30 m pixels (Figure 4d-f),

378 but the capacity to distinguish community

379 types has largely broken down at 90 m

380 (Figure 4g-i).

381 The trends were similar between

382 analyses using 50 spectral species versus 20

383 spectral species. However, the 20

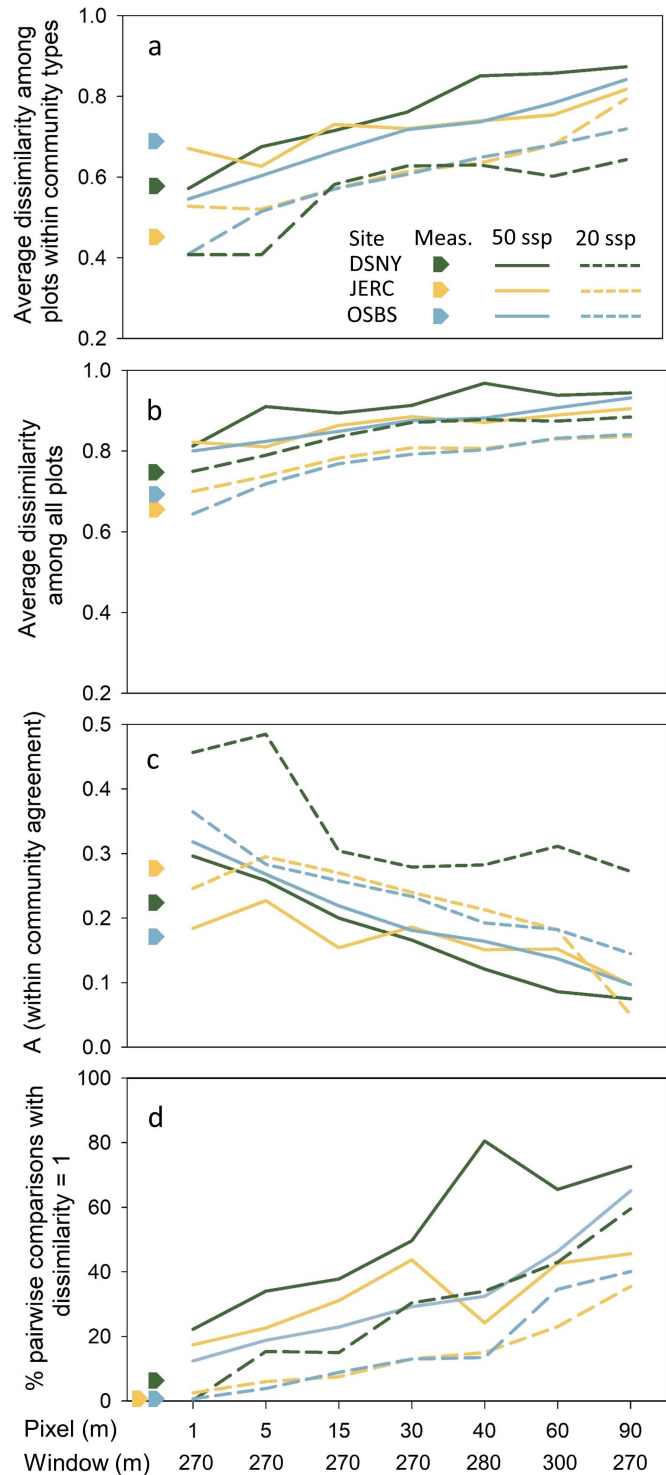


Figure 3. Spectral species dissimilarity within community types, dissimilarity among all plot locations, within community agreement (A), and percentage of comparisons with absolute disagreement for each pixel resolution, study site, and 50 versus 20 spectral species using 270-300 m mapping windows. Symbols represent values for field-measured plots using actual plant species.

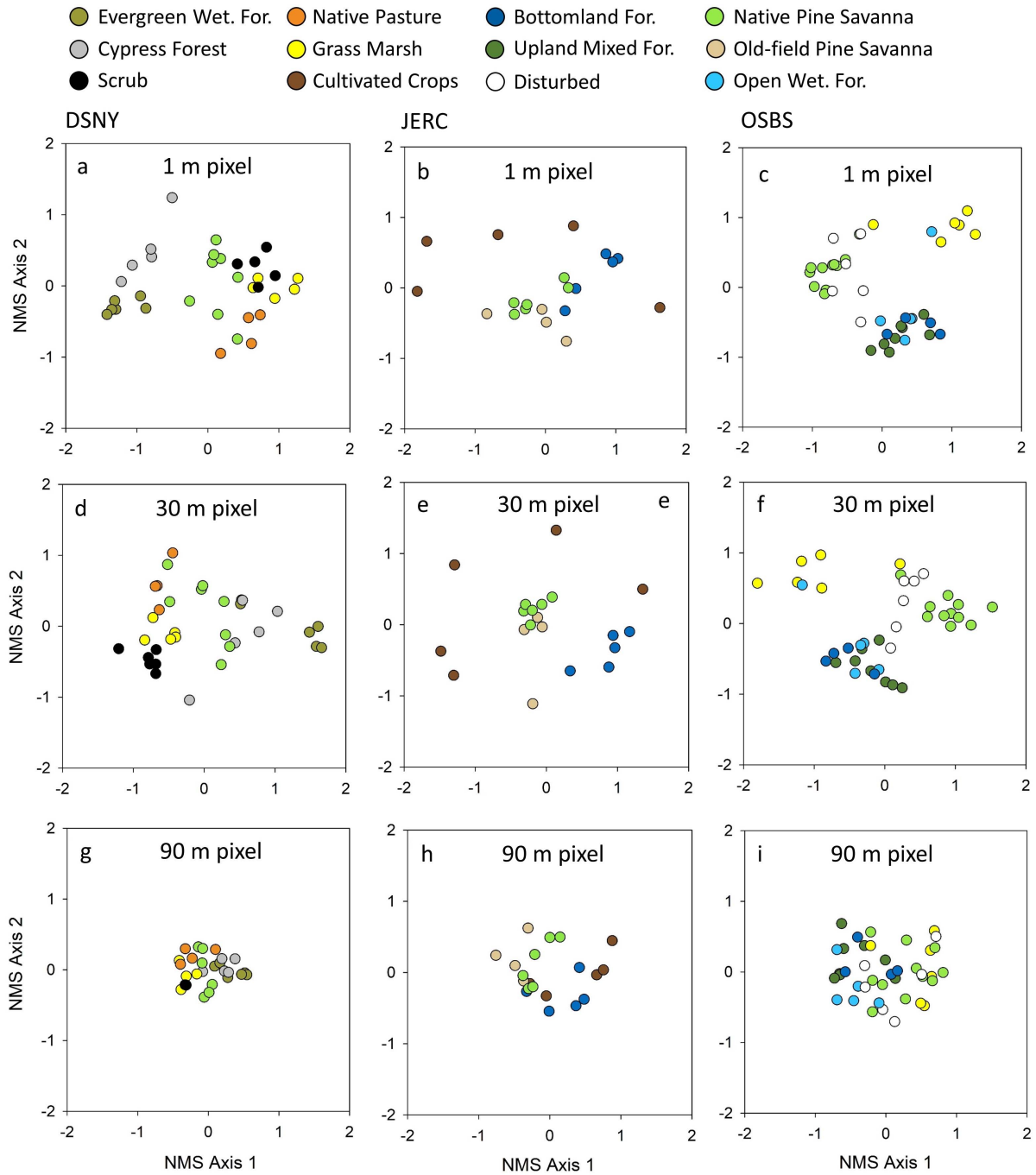


Figure 4. Results from NMS analyses from Bray-Curtis dissimilarity matrices generated by biodivMapR at using three pixel resolutions (1m, 30 m, 90 m) and 270 m mapping windows using 50 spectral species at each of the three study sites (DSNY = Disney Wilderness Preserve, JERC = Jones Ecological Research Center, OSBS = Ordway-Swisher Biological Research Station). Symbol colors correspond to community types.

385 spectral species invariably resulted in
 386 lower dissimilarity among plots, higher
 387 within community agreement, and fewer
 388 pairwise comparisons with dissimilarity =
 389 1, and thus overall higher resolution in
 390 distinguishing plots among community
 391 types (Figure 3a-d).

392 Field measured values for
 393 dissimilarity metrics were generally most
 394 similar to remote sensing estimates that
 395 used the finest pixel resolution (Figure 3a-
 396 d). Field-measured plots had very few
 397 pairwise comparisons with zero plant
 398 species in common, in sharp contrast to
 399 virtual plot dissimilarities based on
 400 spectral species (Figure 3d).

401 For our second analysis, which
 402 compared varying pixel resolutions and
 403 mapping window sizes with similar
 404 numbers of pixels per window (49-81),
 405 there were no strong trends evident
 406 (Figure 5a-d). The values were generally
 407 similar to those for intermediate pixel

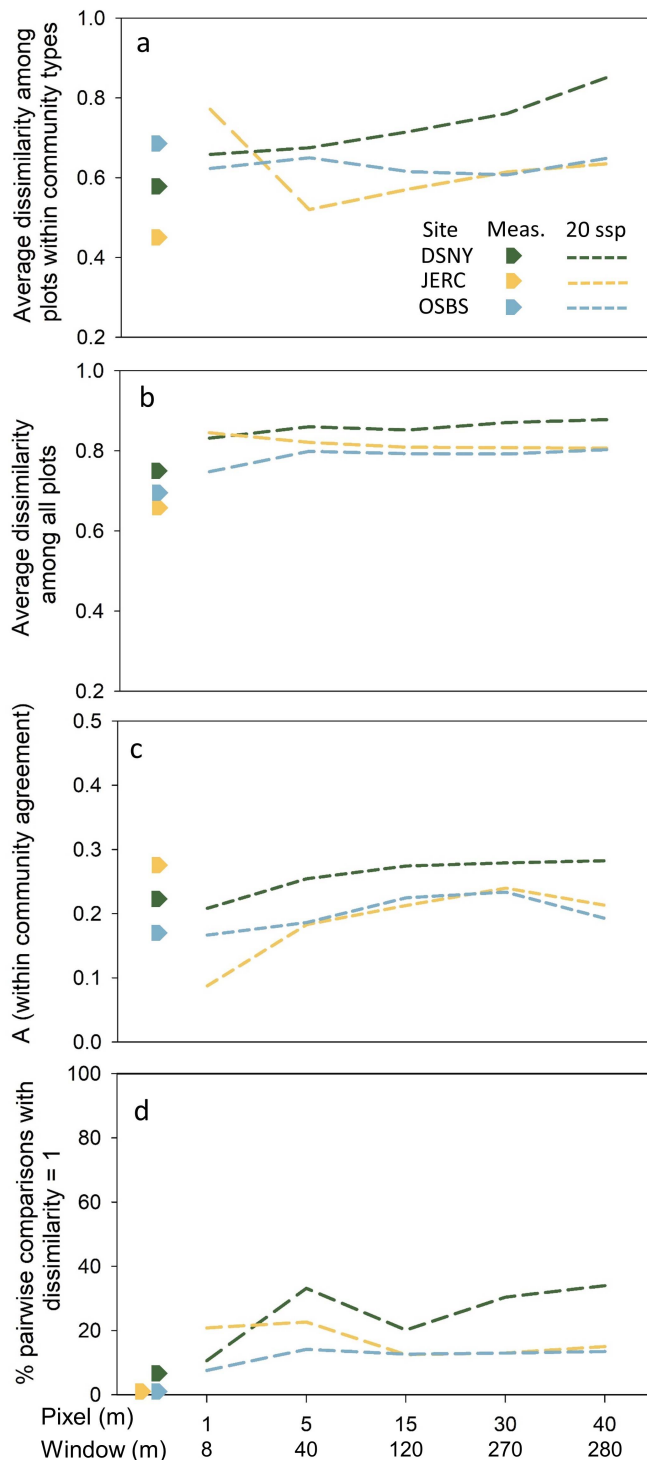


Figure 5. Spectral species dissimilarity within community types, dissimilarity among all plot locations, within community agreement (A), and percentage of comparisons with absolute disagreement for each pixel resolution and study site using 20 spectral species and varying sized mapping windows with 49-81 spectral species per window. Symbols represent values for field-measured plots using actual plant species.

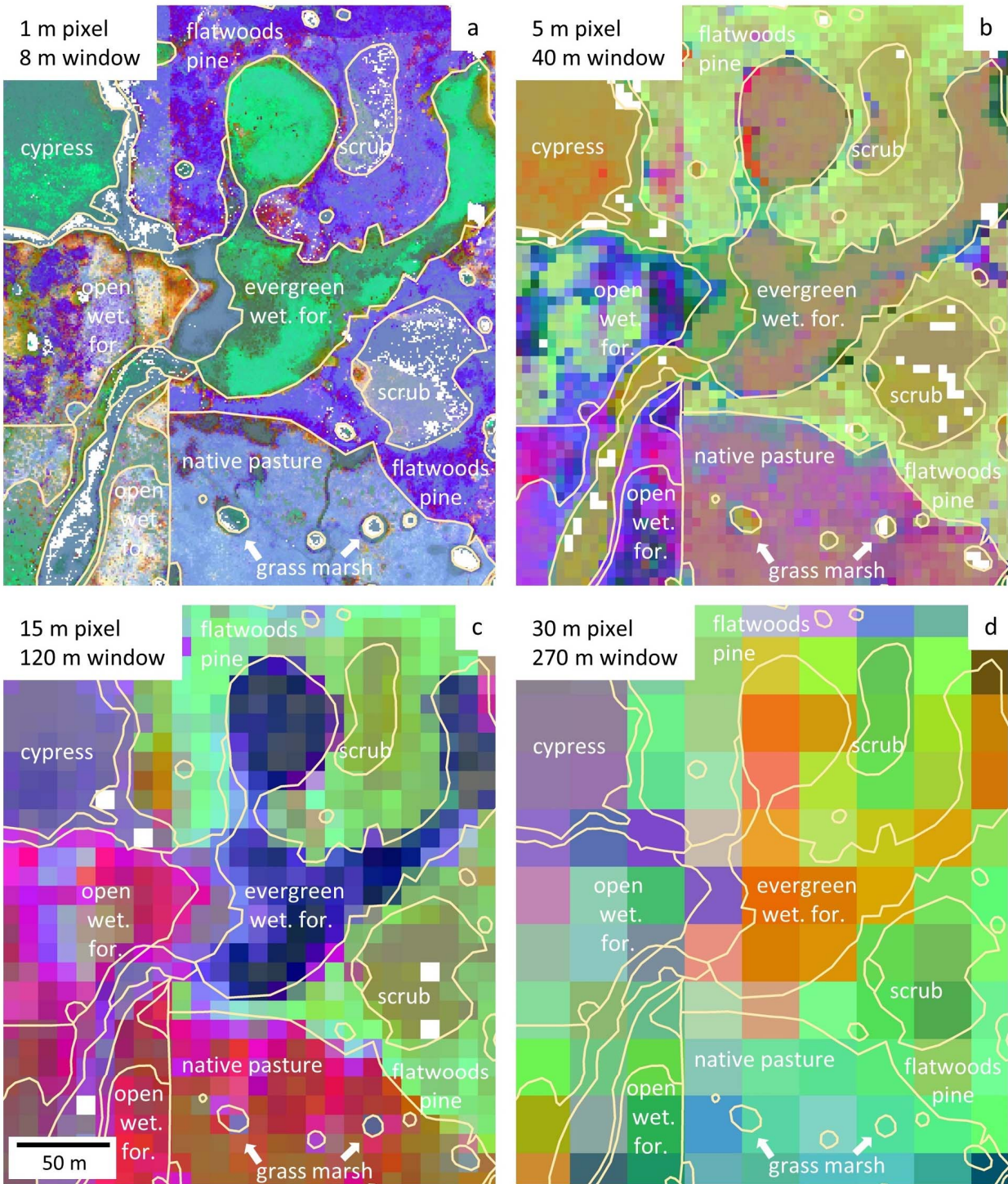


Figure 6. Beta diversity maps generated by bioDivMapR using different pixel resolutions and mapping window sizes to represent part of the Disney Wilderness Preserve (DSNY). Beige lines indicate the extent of natural community types interpreted from aerial photographs, and some natural community types are labeled.

408

409

resolutions (30-40 m) using the 270-300 m mapping windows (Figure 3a-d).

410 Taken together, these results show that the number of pixels per window has the strongest
411 influence on ability to discern community types using biodivMapR. However, beta diversity
412 maps generated from varying window sizes with similar numbers of pixels per window show that
413 increasing window size to incorporate more pixels decreases the spatial resolution of beta
414 diversity maps, which at some point decreases the capacity to spatially distinguish community
415 types (Figure 6a-d).

416 **4 Discussion**

417 4.1 Assessment of biodivMapR outputs

418 Results of our analysis indicate that spatial resolution of imagery has a strong effect on
419 the capacity to identify beta diversity using the algorithm biodivMapR. The key variable
420 influencing the ability to detect relative levels of dissimilarity among locations is the number of
421 pixels per mapping window, where more pixels provide greater resolution. Increasingly coarse
422 pixel resolution can be compensated by increasing the mapping window size, though at the cost
423 of decreasing spatial resolution of beta diversity maps built from the windows.

424 The decreasing capacity to identify beta diversity with fewer pixels per mapping unit
425 appears to result primarily from overestimation of dissimilarity among mapping windows within
426 community types, such that there is a loss of distinction between the within-community
427 dissimilarity and total dissimilarity. This overestimation results from pairwise comparisons
428 between windows showing increasingly few or zero spectral species in common as pixels per
429 window decreases, even if comparisons are within the same community type. Where there were
430 fewer than 50 pixels per mapping window (60-90 m pixels within 270-300 m mapping
431 windows), more than half of the total dissimilarities were equal to one (Figure 3d). Such absolute
432 dissimilarities provide limited information, even if between different community types, as they

433 suggest that communities within the same landscape have no more species in common than
434 communities on different continents. In fact, however, all pairwise comparisons among
435 community types using field data at JERC and OSBS showed at least some generalist species in
436 common, and only about 6% of comparisons at DSNY had no species in common. We suggest
437 that using the appropriately sized mapping window relative to image pixel size, particularly with
438 the goal of minimizing the number of dissimilarities equal to one, is essential for producing the
439 most meaningful beta diversity maps. The recommendation by Féret and de Boissieu (2020) that
440 there be a minimum of 50 pixels per mapping window seems appropriate, although, as they point
441 out, assigning an appropriate number of spectral species is also important.

442 The strong effect of number of spectral species on detection of beta diversity also relates
443 to overestimation of dissimilarity in pairwise comparisons among mapping windows. In this
444 study, reducing the number of spectral species from 50 to 20 considerably improved the capacity
445 to distinguish community types. This effect may seem counterintuitive, but reducing the number
446 resulted in there being more spectral species in common among windows within community
447 types, which more strongly contrasted average dissimilarity among all community types. The
448 advantage of having fewer spectral species may be a special case where pixels represent local
449 plant community composition rather than individual plant species. Where two pixels are assigned
450 different spectral species when in fact they have some species in common, their dissimilarity is
451 overestimated as 1 (Rocchini et al., 2022). For the studied community types, it is easy to imagine
452 that variations in the local abundance of potentially high-cover species, such as wiregrass,
453 longleaf pine, and saw palmetto, might cause different spectral species classifications despite the
454 overall plant community composition is quite similar (Ostertag and Robertson, 2007). Of course
455 at some point reduction of spectral species will cause pixels classifications to be overly

456 homogenized and will not effectively represent degree of dissimilarity among communities.
457 Currently the appropriate number of spectral species must be determined by trial and error with
458 validation data, but eventually better guidelines might be determined based on the spatial
459 resolution of imagery relative to the spatial scale of plant community complexity.

460 4.2 Implications for the SBG mission

461 Our results indicate the importance of maximizing the spatial resolution of imagery for
462 the most effective mapping and monitoring of biodiversity. Using `biodivMapR` or similar
463 algorithms, the spatial resolution of imagery will determine the minimum size of mapping
464 windows with enough pixels to produce meaningful maps, which in turn limits the spatial
465 resolution of those maps. The implications of mapping window size depend on the spatial
466 distribution of natural community types representing plant beta diversity on a given landscape. In
467 the southeastern U.S. Coastal Plain, pixel resolutions ≥ 30 m, such as those recommended for the
468 SBG mission, corresponding to mapping windows > 270 m in order to contain > 50 pixels,
469 would be insufficient for identifying the contribution to beta diversity by certain community
470 types, such as isolated ephemeral ponds and narrow riparian features. However, coarser
471 resolution data might still identify beta diversity among larger ecological features, such areas
472 dominated by native pine communities, scrub, cypress forests, and native pastures (Figure 6).

473 Our study provides some context for assessing tradeoffs in investment among image
474 spatial resolution, spectral resolution, signal-to-noise ratio, and flyover return interval. Although
475 our focus was on spatial resolution, the ability for `biodivMapR` to distinguish natural community
476 types as well as it did even with much coarser spatial resolution than those generally
477 recommended for remote sensing of biodiversity (Gamon et al., 2020) presumably benefited
478 from the immense spectral resolution afforded by hyperspectral imagery (Thorpe et al., 2013).

479 Flights for the NEON project were chosen on clear days, whereas utility of satellite remote
480 sensing data is limited by cloudiness, underscoring the importance of sufficiently frequent
481 returns to collect cloud-free data in regions where clear days are limited. Data acquisition at a
482 frequency sufficient to account for seasonal effects and plant phenological changes and to
483 monitor changes in land use and ecological status over time is also critical. For example,
484 analyses in this study were simplified by having full coverages of the areas of interest within a
485 few days and at the height of the growing season. However, within these limits, our analysis
486 underscores the need to maximize the spatial resolution of imagery for effective mapping of
487 plant beta diversity.

488

489 **5 Conclusions**

490 Using the algorithm biodivMapR with hyperspectral remote sensing imagery, we show
491 that the capacity to detect plant beta diversity as represented by plant community types decreases
492 with number of pixels per mapping window. It follows that pixel resolution places a lower limit
493 on size of mapping windows that are effective for distinguishing community types, which in turn
494 limits the spatial resolution beta diversity maps composed of mapping windows. When image
495 pixel size is much larger than individual plants, the effect of having too few pixels per window,
496 as well as assignment of too many spectral species per image, has the effect of overestimating
497 dissimilarity among locations that in fact may have many plant species in common. This
498 overestimation undermines the capacity to contrast mapping window dissimilarity within versus
499 among community types and thus reduces the information content of beta diversity maps. These
500 results demonstrate the advantage of maximizing spatial resolution of hyperspectral imaging
501 instruments on the anticipated NASA Surface Biology and Geology satellite mission and similar

502 remote sensing projects.

503

504 **Acknowledgments**

505 Funding for the project was provided by NASA grant 80NSSC21K1956 and Tall Timbers
506 Research Station. The National Science Foundation National Ecological Observatory Network
507 (NEON) provided remote sensing imagery and plot field data on which the study was based. We
508 thank Beatriz Pace-Aldana of The Nature Conservancy Disney Wilderness Preserve, Jeffery
509 Cannon of the Jones Ecological Research Center, and Andrew Rappe of Ordway-Swisher
510 Biological Station for providing access to sites and support for field work. We thank Joe Noble
511 and Morgan Varner for administrative and technical support.

512

513 **Open Research**

514 Software used in analyses were:

515 PC-ORD, citation McCune, B., & Mefford, M. J. (2018) *PC-ORD. Multivariate Analysis of*
516 *Ecological Data v. 7.08*. Oregon: MjM Software Design, available for download at
517 <https://www.wildblueberrymedia.net/store/pc-ord-7-single-user-license-regular-new-user>.

518 R, downloadable at <https://www.r-project.org/>. We specifically used package version 2.6-2.

519 <https://doi.org/10.1002/env.516> <https://CRAN.R-project.org/package=vegan>>

520 BiodivMapR was downloaded from <https://github.com/jbferet/biodivMapR> and installed
521 with the command line devtools::install_github('https://github.com/jbferet/biodivMapR.git') as
522 provided in the manuscript by Asner and de Boissieu (2020). Data command were those
523 described in the manuscript text.

524

525 Data sources are described as follows:

526 NEON hyperspectral remote sensing data as described in the manuscript was accessed by
527 logging into the NEON data portal (<https://data.neonscience.org/home>), where the user can
528 browse to or search for the section called Spectrometer orthorectified surface directional
529 reflectance - mosaic, where available data are listed by date for each NEON site.

530 NEON plant presence and percent cover as described in the manuscript was accessed by
531 logging into the NEON data portal (<https://data.neonscience.org/home>), where the user can
532 browse to or search for the section called Plant presence and percent cover, where data for each
533 site are displayed for download.

534 The Bray-Curtis dissimilarity matrices for all analyses presented, and the shapefiles of field
535 plot and virtual plot locations to which the matrices pertain, have been submitted for open access
536 storage in Pangaea (pangaea.de). The data submission is pending review.

537

538 **References**

539 Carr, S. C., Robertson, K. M., & Peet, R. K. (2010) A vegetation classification of fire-dependent
540 pinelands of Florida. *Castanea*, 75(2), 153-189. <https://doi.org/10.2179/09-016.1>

541 Cavender-Bares, J., Gamon, J. A., & Townsend, P. A. (2020) The use of remote sensing to
542 enhance biodiversity monitoring and detection: A critical challenge for the twenty-first
543 century. In J. Cavender-Bares, J. A. Gamon, P. A. Townsend (Eds.), *Remote sensing of plant*
544 *biodiversity* (pp. 1-12). Cham, Switzerland: Springer.

545 Cawse-Nicholson, K., Townsend, P. A., Schimel, D., Assiri, A. M., Blake, P. L., Buongiorno, M.
546 F., Campbell, P., Carmon, N., Casey, K. A., Correa-Pabón, R. E. & Dahlin, K.M. (2021)
547 NASA's surface biology and geology designated observable: A perspective on surface

548 imaging algorithms. *Remote Sensing of Environment*, 257, 112349.
549 <https://doi.org/10.1016/j.rse.2021.112349>

550 Dixon, C. M., Robertson, K. M., Ulyshen, M. D., & Sikes, B. A. (2021) Pine savanna restoration
551 on agricultural landscapes: The path back to native savanna ecosystem services. *Science of*
552 *the Total Environment*, 818, 151715. <https://doi.org/10.1016/j.scitotenv.2021.151715>

553 Drewa, P. B., Platt, W. J., & Moser, E. B. (2002) Community structure along elevation gradients
554 in headwater regions of longleaf pine savannas. *Plant Ecology*, 160(1), 61-78.
555 <https://doi.org/10.1023/A:1015875828742>

556 Féret, J.-B. & Asner, G. P. (2014) Mapping tropical forest canopy diversity using high-fidelity
557 imaging spectroscopy. *Ecological Applications*, 24(6), 1289-1296.
558 <https://doi.org/10.1890/13-1824.1>

559 Féret, J. B., & de Boissieu, F. (2020) biodivMapR: An R package for α -and β -diversity mapping
560 using remotely sensed images. *Methods in Ecology and Evolution*, 11(1), 64-70.
561 <https://doi.org/10.1111/2041-210X.13310>

562 Florida Natural Areas Inventory. (2010) *Guide to the natural communities of Florida: 2010*
563 *edition*. Tallahassee, Florida: Florida Natural Areas Inventory.

564 Gamon, J. A., Wang, R., Gholizadeh, H., Zutta, B., Townsend, P. A., & Cavender-Bares, J..
565 (2020) Chapter 16: Consideration of scale in remote sensing of biodiversity. In J. Cavender-
566 Bares, J. A. Gamon, P. A. Townsend (Eds.), *Remote sensing of plant biodiversity* (pp. 425-
567 447). Cham: Springer.

568 Gholizadeh, H., Gamon, J. A., Townsend, P. A., Zygielbaum, A. I., Helzer, C. J., Hmimina, G.
569 Y., Yu, R., Moore, R. M., Schweiger, A. K., & Cavender-Bares, J. (2019) Detecting prairie

570 biodiversity with airborne remote sensing. *Remote Sensing of Environment*, 221, 38-49.
571 <https://doi.org/10.1016/j.rse.2018.10.037>

572 Gholizadeh, H., Gamon, J. A., Helzer, C. J., & Cavender-Bares, J. (2020) Multi-temporal
573 assessment of grassland α -and β -diversity using hyperspectral imaging. *Ecological*
574 *Applications*, 30(7), e02145. <https://doi.org/10.1002/eap.2145>

575 Glitzenstein, J. S., Streng, D. R., & Wade, D. D. (2003) Fire frequency effects on longleaf pine
576 (*Pinus palustris* P. Miller) vegetation in South Carolina and Northeast Florida, USA.
577 *Natural Areas Journal*, 23(1), 22-37.

578 Karpowicz, B., & Kampe, T. (2015) The NEON imaging spectrometer radiance to reflectance
579 algorithm theoretical basis document. NEON document #NEON.DOC.001288. Boulder,
580 Colorado: National Ecological Observation Network, National Science Foundation.
581 <https://data.neonscience.org/data-products/DP3.30006.001#collectionAndProcessing>

582 Kirkman, L. K., Coffey, K. L., Michell, R. J., & Moser, E. B. (2004) Ground cover recovery
583 patterns and life-history traits: implications for restoration obstacles and opportunities in a
584 species-rich savanna. *Journal of Ecology*, 92(3), 409-421. [https://doi.org/10.1111/j.0022-](https://doi.org/10.1111/j.0022-0477.2004.00883)
585 [0477.2004.00883](https://doi.org/10.1111/j.0022-0477.2004.00883).

586 Lane, C. R., & D'Amico, E. (2010) Calculating the ecosystem service of water storage in
587 isolated wetlands using LiDAR in north central Florida, USA. *Wetlands*, 30, 967-977.
588 [doi:10.1007/s13157-010-0085-z](https://doi.org/10.1007/s13157-010-0085-z)

589 Lortie, C. J., Brooker, R. W., Choler, P., Kikvidze, Z., Michalet, R., Pugnaire, F. I., & Callaway,
590 R. M. (2004) Rethinking plant community theory. *Oikos*, 107(2), 433-
591 438. <https://doi.org/10.1111/j.0030-1299.2004.13250.x>

592 McCune, B., & Grace, J. B. (2002) *Analysis of ecological communities*. Glenden Beach,
593 Oregon: MjM Software Design.

594 McCune, B., & Mefford, M. J. (2018) *PC-ORD. Multivariate Analysis of Ecological Data v.*
595 *7.08*. Oregon: MjM Software Design.

596 National Academies of Sciences, Engineering, and Medicine (2018) *Thriving on our changing*
597 *planet: A decadal strategy for earth observation from space*. Washington, DC: The National
598 Academies Press. <https://doi.org/10.17226/24938>

599 NEON (National Ecological Observatory Network). *Plant presence and percent cover*
600 (DP1.10058.001), RELEASE-2022. <https://doi.org/10.48443/pr5e-1q60>. Dataset accessed
601 from <https://data.neonscience.org> on June 28, 2022

602 Noss, R. F., Platt, W. J., Sorrie, B. A. Sorrie, Weakley, A. S., Means, D. B., Costanza, J., & Peet,
603 R. K. (2015) How Global Biodiversity Hotspots May Go Unrecognized: Lessons from the
604 North American Coastal Plain. *Diversity and Distributions*, 21(2), 236–244.
605 <https://doi.org/10.1111/ddi.12278>

606 Oksanen, J., Simpson, G., Blanchet, F., Kindt, R., Legendre, P., Minchin, P., O'Hara, R.,
607 Solymos, P., Stevens, M., Szoecs, E., Wagner, H., Barbour, M., Bedward, M., Bolker, B.,
608 Borcard, D., Carvalho, G., Chirico, M., De Caceres, M., Durand, S., Evangelista, H., Fitz, J.
609 R, Friendly, M., Furneaux, B., Hannigan, G., Hill, M., Lahti, L., McGlinn, D., Ouellette, M.,
610 Ribeiro, Cunha, E., Smith, T., Stier, A., Ter Braak, C., Weedon, J. (2022) `_vegan:`
611 `Community Ecology Package_`. R package version 2.6-2. <https://doi.org/10.1002/env.516>
612 <https://CRAN.R-project.org/package=vegan>>

613 Ostertag, T. E., & Robertson, K. M. (2007) A comparison of native versus old-field vegetation in
614 upland pinelands managed with frequent fire, South Georgia, USA. *Tall Timbers Fire*
615 *Ecology Conference Proceedings*, 23. 109-120.

616 Palmer, M. W., Earls, P. G., Hoagland, B. W., White, P. S., & Wohlgemuth, T. (2002).
617 Quantitative tools for perfecting species lists. *Environmetrics*, 13, 121–137.
618 <https://doi.org/10.1002/env.516>

619 Pereira, H. M., Belnap, J., Böhm, M., Brummitt, N., Garcia-Moreno, J., Gregory, R., Martin, L.,
620 Peng, C., Proença, V., Schmeller, D. and Swaay, C. V. (2017) Monitoring essential
621 biodiversity variables at the species level. In *The GEO handbook on biodiversity observation*
622 *networks* (pp. 79-105). Cham, Switzerland: Springer.

623 Picotte, J. J., & Robertson, K. M. (2011) Timing constraints on remote sensing of wildland fire
624 burned area in the southeastern US. *Remote Sensing*, 3(8), 1680-1690.
625 <https://doi.org/10.3390/rs3081680>

626 Robertson, K. M., Platt, W. J., & Faires, C. E. (2019) Patchy fires promote regeneration of
627 longleaf pine (*Pinus palustris* Mill.) in pine savannas. *Forests* 10(5), 367.
628 <https://doi.org/10.3390/f10050367>

629 Rocchini, D., Chiarucci, A., & Loiselle, S. A. (2004) Testing the spectral variation hypothesis by
630 using satellite multispectral images. *Acta Oecologica*, 26(2), 117-120.
631 <https://doi.org/10.1016/j.actao.2004.03.008>

632 Rocchini, D., Balkenhol, N., Carter, G.A., Foody, G.M., Gillespie, T.W., He, K.S., Kark, S.,
633 Levin, N., Lucas, K., Luoto, M., & Nagendra, H. (2010) Remotely sensed spectral
634 heterogeneity as a proxy of species diversity: recent advances and open

635 challenges. *Ecological Informatics*, 5(5), 318-329.
636 <https://doi.org/10.1016/j.ecoinf.2010.06.001>

637 Rocchini, D., Luque, S., Pettorelli, N., Bastin, L., Doktor, D., Faedi, N., Feilhauer, H., Feret,
638 J.B., Foody, G.M., Gavish, Y., & Godinho, S. (2018) Measuring β -diversity by remote
639 sensing: a challenge for biodiversity monitoring. *Methods in Ecology and Evolution*, 9(8),
640 1787–1798. <https://doi.org/10.1111/2041-210X.12941>

641 Schimel, D., Townsend, P. A., & Pavlick, R. (2020) Prospects and pitfalls for spectroscopic
642 remote sensing of biodiversity at the global scale. In J. Cavender-Bares, J. A. Gamon, P. A.
643 Townsend (Eds.), *Remote sensing of plant biodiversity* (pp. 503-518). Cham, Switzerland:
644 Springer.

645 Soil Survey Staff, National Resources Conservation Service, USDA. 2022 *Web soil survey*.
646 <https://websoilsurvey.nrcs> (accessed 30 September 2022)

647 Sousa, D., Brodrick, P., Cawse-Nicholson, K., Fisher, J. B., Pavlick, R., Small, C., & Thompson,
648 D.R. (2022) The Spectral Mixture Residual: A source of low-variance information to
649 enhance the explainability and accuracy of surface biology and geology Retrievals. *Journal*
650 *of Geophysical Research: Biogeosciences*, 127(2), p.e2021JG006672.
651 <https://doi.org/10.1029/2021JG006672>

652 Thorp, K. R., French, A. N., & Rango, A. (2013). Effect of image spatial and spectral
653 characteristics on mapping semi-arid rangeland vegetation using multiple endmember
654 spectral mixture analysis (MESMA). *Remote Sensing of Environment*, 132, 120–130.
655 <https://doi.org/10.1016/j.rse.2013.01.008>
656
657